Supporting Information for: Large-area, Highly Uniform Evaporated Formamidinium Lead Triiodide Thin-films for Solar Cells

Juliane Borchert, Rebecca L. Milot, Jay B. Patel, Christopher L. Davies, Adam D. Wright, Laura Martínez Maestro, Henry J. Snaith, Laura M. Herz, and Michael B. Johnston*

Clarendon Laboratory, Department of Physics, University of Oxford, Parks Road, OX1 3PU, United Kingdom

E-mail: michael.johnston@physics.ox.ac.uk

Device Fabrication

Co-evaporation was used to fabricate formamidinium lead triiodide based solar cells. We fabricated both neat $FAPbI_3$ thin films for characterization and complete solar cells to measure the solar cell performance.

In a modified Kurt J. Lesker dual source evaporation system, PbI_2 and FAI were heated in separate crucibles until each of them evaporated. During evaporation the pressure in the chamber was 10^{-6} mbar. The evaporation temperature for FAI was 150 °C, and PbI_2 was evaporated at 300 °C. The vapors condensed on rotating substrates. The rotation helps ensure uniform coating. To obtain thin-films for PL spectroscopy, THz spectroscopy, ultraviolet-visible spectroscopy and infrared spectroscopy this deposition was carried out on z-cut quartz or KBr crystals as substrates. All $FAPbI_3$ layers were annealed at 170 °C for 1 min.

The solar cells were fabricated on a fluoride-doped tin oxide (FTO) coated glass substrate. A commercially available glass substrate from Pilkington with a trade name "TEC15" was used. The FTO was cleaned using a multi-step cleaning protocol that involved scrubbing with Hellmanex solution, sonicating in acetone and isopropanol and cleaning with oxygen plasma. C_{60} was evaporated onto these clean FTO substrates in the same evaporation system which was used for the perovskite deposition. C_{60} with a purity of 99.9 % was bought from Acros Organics and evaporated at 350° C.[1] The perovskite layer was deposited onto this as described above. Next, 2,2',7,7'-Tetrakis-(N,N-di-4-methoxyphenylamino)-9,9'-spirobifluorene (Spiro-OMeTAD) from Lumtec was spin-coated as the hole extraction layer. Spiro-OMeTAD was doped with Lithium bis(trifluoromethanesulfonyl)imide (LiTFSI) and 4-tert-Butylpyridine (tBP) and spin coated at 2000 rpm for 45 s. Finally, 100 nm of silver were evaporated in a second evaporation chamber to complete the solar cells. The size of the evaporated metal contacts defined the area of the solar cells as 0.0919 cm^2.

The vacuum chamber which was used for the perovskite evaporation had previously been used for the evaporation of various other materials including methylammonium iodide (MAI), lead

chloride ($PbCl_2$) and fullerenes. To assess if this had lead to contamination, we performed infrared spectroscopy (Figure 3b). We found that the characteristic features of $FAPbI_3$ are present: the peak at $1713\,cm^{-1}$ matches the C=N stretch in the FA^+ cation and the peaks at $3269\,cm^{-1}$ and $3406\,cm^{-1}$ correspond to the N-H stretching vibrations.[2,3] Additionally, in the visible range of the spectrum around 1.5 eV the film starts absorbing the incident light. This is consistent with the previously reported values for the absorption onset in solution processed $FAPbI_3$.[4] Both the infrared and visible absorption measurements show that we did successfully deposit $FAPbI_3$ and did not see a significant amount of contamination from materials previously deposited in the same vacuum chamber.

Device characterization

To characterize the solar cells, current-voltage (J–V) sweeps and stabilized power output measurements were carried out. An ABET class AAB sun 2000 simulator was used to simulate an AM 1.5 light spectrum. The scan speed was $0.38\,Vs^{-1}$. Black metal masks were used to define the active area and prevent influences from scattered light. To measure the stabilized power output, we held the cells close to the maximum power point for 50 s to see how the cells stabilized under typical working conditions.

Additionally, we measured the external quantum efficiency (EQE) using the same Bruker Vertex 80v interferometer used for the IR and visible spectra. A Fourier transform photo current spectroscopy approach,[5] was utilized with a resolution of $100\,cm^{-1}$ and acquisition rate of 5 kHz. Each 341 ms scan was repeated 50 times. A Newport Oriel Sol3A class AAA solar simulator was used as the light source and the solar cell acted as the detector. A Newport calibrated silicon reference solar cell was used as the reference.

Film and Material characterization

To learn more about the properties of the deposited perovskite thin-films and the material itself, we utilized various characterization techniques.

Firstly, X-ray diffraction patterns were measured using a Panalytical X'pert powder diffractometer with a copper X-ray source.

For the PL measurements the sample was mounted in a vacuum cell ($p < 10^{-2}$ mbar) and photoexcited by a 398 nm picosecond pulsed diode laser (PicoHarp, LDH-D-C-405M). The resultant photoluminescence (PL) was collected and coupled into a grating spectrometer (Princeton Instruments, SP-2558), which directed the spectrally dispersed PL onto either an iCCD (PI-MAX4, Princeton Instruments) or a photon-counting detector (PDM series from MPD), whose timing was controlled with a PicoHarp300 TCSPC event timer. The PL spectrum was measured by the iCCD, under continuous wave excitation with an intensity of 100 mWcm^{-2}. The PL time decay data were measured at a wavelength of 800 nm, under an excitation fluence of 1 nJcm^{-2} and a pulse repetition rate of 1 MHz. To allow for easier comparison of our PL lifetime results PL lifetimes which have been reported in the literature for solution processed $FAPbI_3$ are given in table 1.

Table 1: PL lifetimes from the literature

	Excitation wavelength	Fluence	Lifetime
Eperon et al.[6]	507 nm	30 nJcm^{-2}	72 ns (holes,) 78 ns (electrons)
Pellet et al.[7]	406 nm		three exponential fit 17 ns, 76 ns, 173 ns
Rehman et al.[8]	400 nm	0.77 μJcm^{-2} and 1.54 μJcm^{-2}	140 ns
This publication	398 nm	1 nJcm^{-2}	2 ns

A Fourier transform infrared spectrometer (Bruker Vertex 80v) was used to measure the reflectance (R) and transmittance (T) spectra of $FAPbI_3$. The following combination of sources and detectors were used to measure the reflectance and transmittance: a tungsten

halogen lamp with a silicon detector for the visible region ($>$ 1.25 eV); a tungsten halogen lamp and a liquid nitrogen-cooled HgCdTe (MCT) detector for the near-infrared (NIR) region (1.25 $>$ E $>$ 0.46 eV); and a global source and MCT detector for the mid-infrared (MIR) region ($<$ 0.46 eV). This data was used to determine the absorption coefficient (α) from the visible to the infrared.

To determine the charge carrier dynamics in these films we conducted optical pump, THz probe measurements. Optical pump/THz probe measurements utilized an amplified laser system (Spectra Physics, Millennia Tsunami Empower Spitfire) with a center wavelength of 800 nm, repetition rate of 1 kHz, average pulse energy of 1 mJ, and pulse duration of 40 fs. Approximately 50 % of the initial power was used to generate and detect THz, and the remaining 50 % was used to photoexcite the sample. THz radiation was generated using optical rectification in a 450 μm thick GaP (110) crystal and detected via free-space electro-optic sampling in a ZnTe chip with 200 μm ZnTe (110) on 3 mm ZnTe (100). The sample was photoexcited at 400 nm following frequency doubling in a β-barium borate (BBO) crystal. The change in peak time-domain THz radiation ($-\Delta$T/T) was monitored as a function of pump-probe delay time in order to determine the charge-carrier dynamics as shown in Figure 4b. All of the measurements were performed with the sample and entire THz beam path in vacuum. The data were fitted using Equation 1, where n is the charge-carrier density, k_3 is the Auger recombination rate constant, k_2 is the bimolecular (electron-hole) recombination rate constant, and k_1 is the monomolecular recombination rate. For the fitting k_3 was set to zero because the excitation fluences were not high enough to measure it. Additionally, k_1 was set according to the rate determined from the PL measurements.

$$\frac{dn}{dt} = -k_3 n^3 - k_2^{\text{apparent}} n^2 - k_1 n \tag{1}$$

Furthermore, atomic force microscopy (AFM) measurements were performed using an Asylum Research MFP-3D atomic force microscope and an ECONO-LTESP-Au tip.

For the scanning transmission electron microscopy (STEM) measurement a thin lamella was prepared using a Carl Zeiss NVision 40 focused ion beam (FIB) with a field emission (FE) scanning electron microscope (SEM) (Gemini column) operated with an accelerating voltages of 5 keV and a short working distance (WD, 3-7 mm) to maximize resolution. The STEM imaging was carried out using a JEOL ARM200F (scanning)-transmission electron microscopes operated at 200 kV in STEM mode. The best micrographs were taken using collection angles from 72.8 to 235.7 mrad. The size of each image is 512x512 and the images were acquired with a dwell time of 18 microseconds/pixel (1.2 s/image).

Profilometer data

Profilometer measurements were performed to assess the uniformity of the deposited large area $FAPbI_3$ thin film shown in Figure 2a. A razor blade was used to scratch away the film in three different areas on the large sample. The scratches in each area were about half a centimeter wide and three centimeters long. The profilometer measurements were performed across the step created by these scratches.

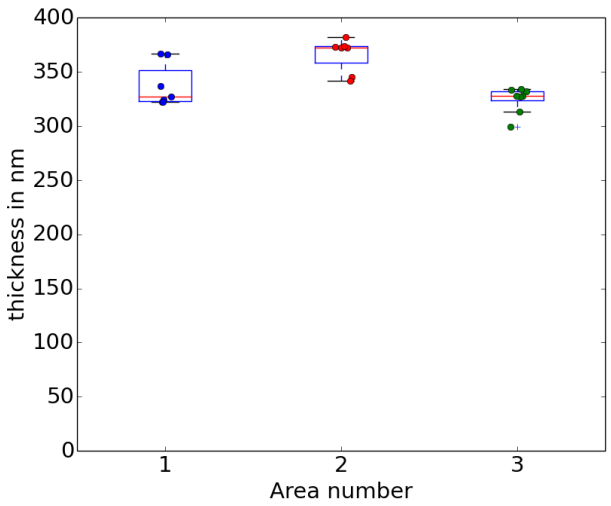

Figure S1: Profilometer measurements were taken in three areas on the film. The bottom left corner (1), the middle (2) and the top right corner (3). In each area several measurements were taken and the median of them was used as the thickness of the film in that area.

Additional atomic force microscopy

In addition to the AFM shown in Figure 2b, we also performed AFM on a bare glass substrate as a comparison to the perovskite film.

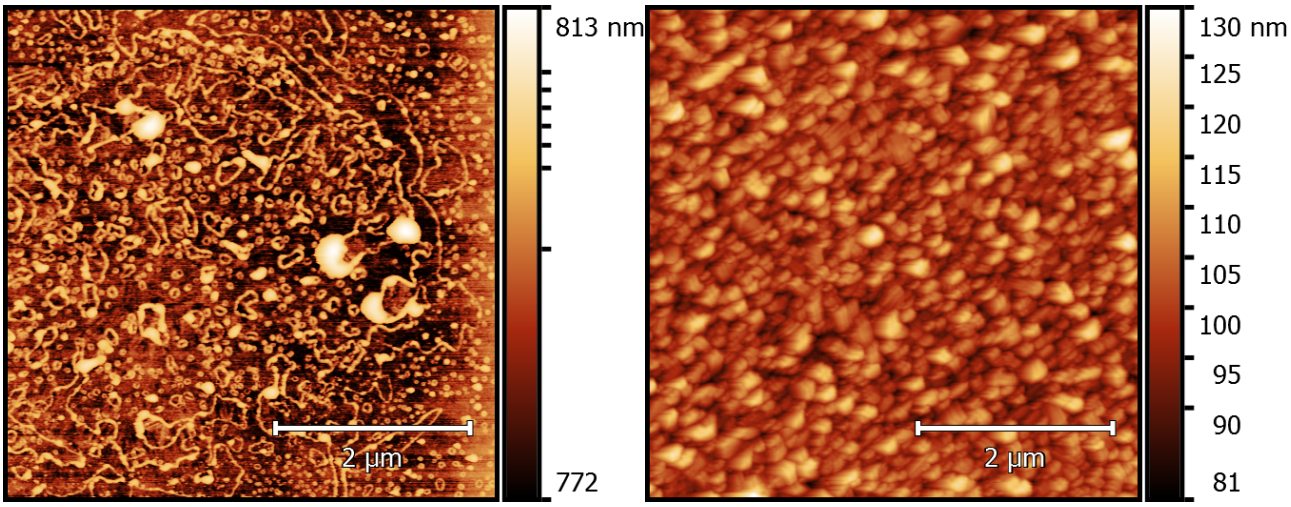

Figure S2: Atomic force microscopy images of the bare glass substrate (left) and the vapor deposited $FAPbI_3$ film. The roughness (R_{RMS}) of the plain glass is 2.7 nm and for the $FAPbI_3$ film it is 6.2 nm.

Scanning electron microscopy

To study the formation of the different layers of the solar cell and their thickness, crosssectional scanning electron microscopy (SEM) was performed. A Hitachi S-4300 field emission scanning electron microscope was used and images were taking with an acceleration voltage of 3 kV. The SEM images showed that the layers of the solar cell were neatly stacked and no holes were found.

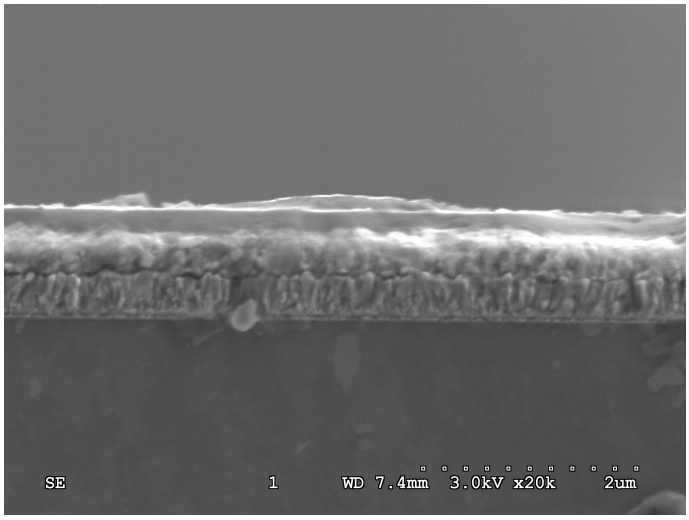

Figure S3: Crossectional scanning electron microscopy image of a $FAPbI_3$ based solar cell. From the bottom the following layers are visible: glass substrate, FTO layer, thin C_{60} layer, $FaPbI_3$ layer and finally a spiro-OMeTAD layer.

Overview over solar cell efficiencies

To give an overview of the overall cell performance, the scanned efficiencies of all the cells of one batch are plotted in a histogram. Many cells show high efficiencies around 14 % and 15 %. The efficiencies from the reverse scans are generally higher than those of the forward scans.

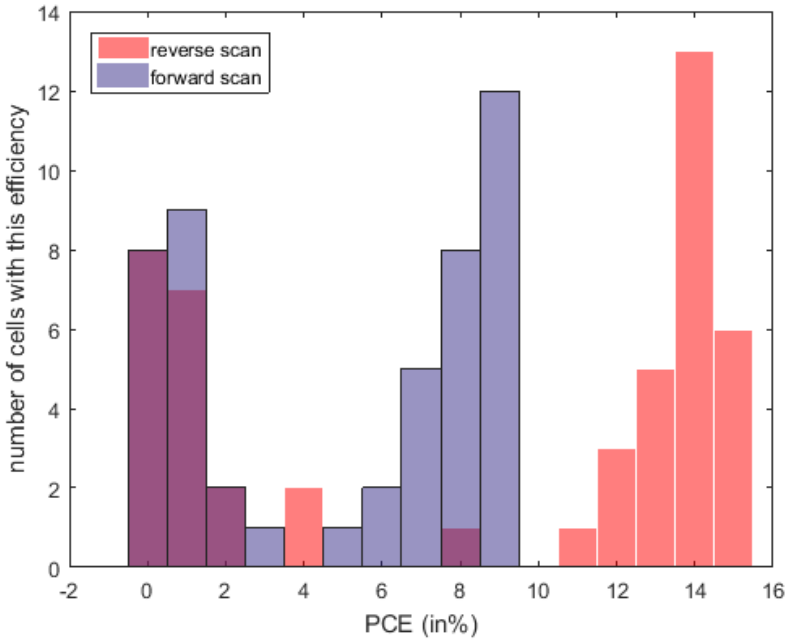

Figure S4: Overview of the efficiency of all cells produced in the same batch as the champion solar cell. Some devices perform very poorly, due to shorting of the device. But a large number of cells reach efficiencies of 14% and 15% in the reverse scan.

For comparison with the literature, power conversion efficiencies of solution processed solar cells containing only $FAPbI_3$ are listed in table 2.

Table 2: Power conversion efficiencies for $FAPbI_3$ solar cells from the literature

Paper	Efficiency	Stabilized
Eperon et al.[6]	14.2 %	no
Lee et al.[9]	14.3 %	no
Wozny et al.[10]	16.4 %	no
Jeon et al.[11]	13.5 %	no
This publication	15.8 %	no
This publication	14.3 %	yes

Phase transition in humid air

When films of $FAPbI_3$ were left in humid air they readily changed color from dark brown to yellow. This indicates a phase transition from the $\alpha - FAPbI_3$ perovskite phase to the non-perovskite $\delta - FAPbI_3$ phase. This transition can be reversed by annealing the film. The large film shown in Figure S5 was left in humid air which triggered this phase transition.

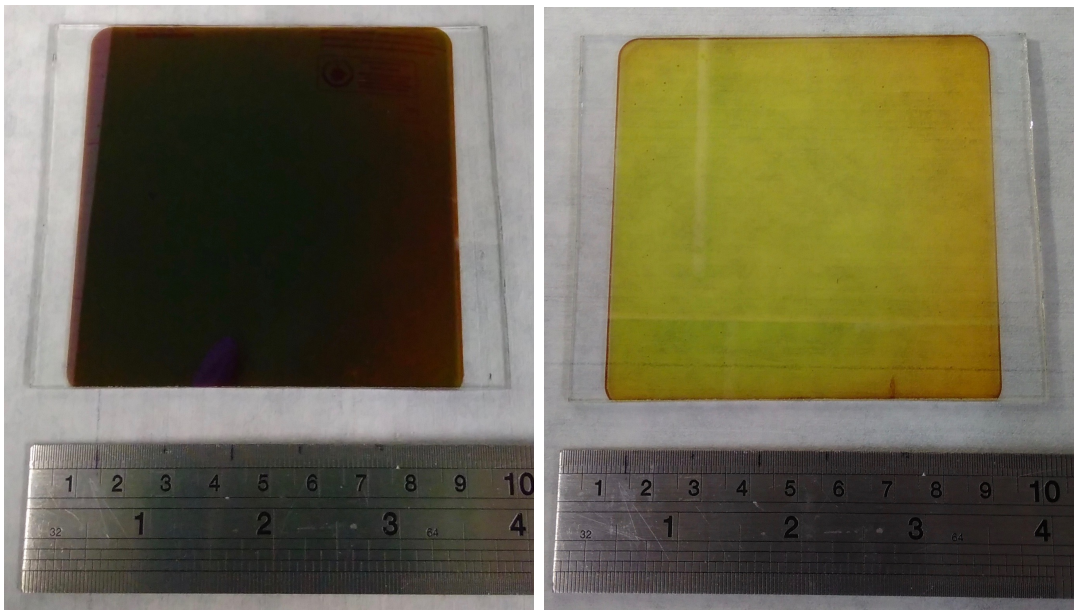

Figure S5: Photographs of the same thin film of $FAPbI_3$ before (left) and after (right) exposure to humid air. The phase transition from the brown perovskite phase to the yellow non-perovskite phase is apparent.

References

(1) Zhao, D.; Ke, W.; Grice, C. R.; Cimaroli, A. J.; Tan, X.; Yang, M.; Collins, R. W.; Zhang, H.; Zhu, K.; Yan, Y. *Nano Energy* **2016**, *19*, 88–97.

(2) Zhou, Z.; Pang, S.; Ji, F.; Zhang, B.; Cui, G. *Chem. Commun.* **2016**, *3828*, 3828–3831.

(3) Dimesso, L.; Quintilla, A.; Kim, Y.-M.; Lemmer, U.; Jaegermann, W. *J. Mater. Sci. Eng. B* **2016**, *204*, 27 – 33.

(4) Koh, T. M.; Fu, K.; Fang, Y.; Chen, S.; Sum, T. C.; Mathews, N.; Mhaisalkar, S. G.; Boix, P. P.; Baikie, T. *J. Phys. Chem. C* **2014**, *118*, 16458–16462.

(5) Vanecek, M.; Poruba, A. *Appl. Phys. Lett.* **2002**, *80*, 719–721.

(6) Eperon, G. E.; Stranks, S. D.; Menelaou, C.; Johnston, M. B.; Herz, L. M.; Snaith, H. J. *Energy Environ. Sci.* **2014**, *7*, 982–988.

(7) Pellet, N.; Gao, P.; Gregori, G.; Yang, T.-Y.; Nazeeruddin, M. K.; Maier, J.; Grätzel, M. *Angew. Chem., Int. Ed. Engl.* **2014**, *53*, 3151–7.

(8) Rehman, W.; Milot, R. L.; Eperon, G. E.; Wehrenfennig, C.; Boland, J. L.; Snaith, H. J.; Johnston, M. B.; Herz, L. M. *Adv. Mater.* **2015**, *27*, 7938–7944.

(9) Lee, J.-W.; Seol, D.-J.; Cho, A.-N.; Park, N.-G. *Advanced Materials* **2014**, *6*, 1–8.

(10) Wozny, S.; Yang, M.; Nardes, A. M.; Mercado, C. C.; Ferrere, S.; Reese, M. O.; Zhou, W.; Zhu, K. *Chemistry of Materials* **2015**, *27*, 4814–4820.

(11) Jeon, N. J.; Noh, J. H.; Yang, W. S.; Kim, Y. C.; Ryu, S.; Seo, J.; Seok, S. I. *Nature* **2015**, *517*, 476–480.